

# Three robust temperature-drift compensation strategies for a MEMS gravimeter

Victor M. Valenzuela,<sup>1</sup> Daniel Teran,<sup>2</sup> Alejandro Sandoval,<sup>2</sup> Eduardo Gomez,<sup>2, a)</sup> John A. Franco-Villafañe,<sup>3</sup> Jesus J. Alcantar-Peña,<sup>4</sup> and Juan Ponce-Hernandez<sup>4</sup>

<sup>1)</sup>*Facultad de Ciencias Físico Matemáticas, Universidad Autónoma de Sinaloa, Sinaloa, 80013,*

*MX*

<sup>2)</sup>*Instituto de Física, Universidad Autónoma de San Luis Potosí, San Luis Potosí, 78295,*

*MX*

<sup>3)</sup>*CONAHCYT - Instituto de Física, Universidad Autónoma de San Luis Potosí, San Luis Potosí, 78295,*

*MX*

<sup>4)</sup>*Centro de Ingeniería y Desarrollo Industrial, Querétaro, 76125, MX*

(Dated: 24 June 2024)

Gravimeters fabricated with MEMS suffer from temperature-dependent drifts in their long-term stability. We analyze the thermal contributions to the signal, and we propose three mechanisms to mitigate their effects. The first one uses materials that fulfill the condition  $\alpha_E = -2\alpha$ , where the thermal expansion is canceled by the temperature variation of the Young's modulus. The second one uses the thermal expansion to introduce a compression that compensates the variation in the force of the spring. In the third one, the expansion compensates the displacement of the proof mass in the sensor, rather than the force. The three mechanisms are robust since they only depend on the temperature of the sensor itself.

## I. INTRODUCTION

Recent progress in precision gravimetry has found extensive applications both in fundamental physics and technology. They appear in proposals to test Non-Newtonian gravity at small scales<sup>1–3</sup>, quantum gravity<sup>4–6</sup> and dark matter detection<sup>7,8</sup>. Applications include inertial navigation<sup>9,10</sup>, monitoring of volcanic activity<sup>11,12</sup>, seismometry<sup>13–15</sup>, exploration of underground resources like water or oil<sup>5,16–18</sup>, and even monitoring climate changes<sup>19,20</sup>.

The gravimeters are divided into absolute and relative. The first ones include the FG5-X gravimeter<sup>21</sup> and those using cold<sup>22–25</sup> or ultra-cold atoms<sup>26,27</sup>. Unfortunately they are expensive and not very practical for field applications due to their weight and complexity, even with the most recent versions<sup>28–34</sup>.

Gravimeters based on micro-electromechanical-system (MEMS) have been gaining importance due to their reliability, low cost and reduced power consumption<sup>35–39</sup>. They measure the displacement  $z$  or the oscillation frequency  $\omega_m$  of a proof mass  $m$  attached to a spring with elastic constant  $k$ . Their drifts can be mitigated by having absolute gravimeters nearby for re-calibration<sup>40–46</sup>. The damping  $\gamma$  determines the ultimate sensitivity and long-term stability, and having a high mechanical quality factor  $Q_m = \omega_m/\gamma$  provides good isolation from environmental noise sources<sup>46–48</sup>. In some gravimeters the mechanical spring is replaced by a magnetically or optically levitated mass<sup>49–55</sup>.

The gravity acceleration is obtained from

$$g = \frac{k}{m}z = \omega_m^2 z. \quad (1)$$

MEMS gravimeters reach a noise floor of about  $1 \mu\text{Gal}/\sqrt{\text{Hz}}$ <sup>56,57</sup>. In the AC (resonant) configuration,  $g$  is measured through a frequency shift  $\Delta\omega_m$ . This method has a high resolution and large range (no displacement limitation)<sup>58–60</sup>, but it requires high quality factors, is more prone to failure by fatigue, and the temperature-dependent frequency drifts limit the long-term stability<sup>61–65</sup>. The DC (static) configuration is easier to implement since  $g$  is obtained from the mass displacement, monitoring the vertical position of a slit located in the test mass. It has good enough resolution and range<sup>37,56,66</sup> to perform state-of-the-art precision gravity measurements and there is much less risk of damage by fatigue since passive structures do not experience sufficient mechanical stress cycles to trigger fatigue<sup>67</sup>.

The long-term stability still requires improvement in MEMS gravimeters, particularly on the temperature sensitivity<sup>68</sup>. Strategies in this direction include temperature stabilization<sup>69–72</sup>, passive compensation through doping<sup>65,73,74</sup>, materials with opposite thermal coefficients<sup>75,76</sup>, differential structure design<sup>60,77,78</sup>, mode-localization<sup>79,80</sup>, engineering the thermal conductance using periodically nanostructured phononic crystals<sup>81–83</sup>, and by compensation of the thermal drift by electrostatically induced pre-stresses on geometric anti-spring structures<sup>84</sup>. In addition to temperature drifts, there is also a pressure dependent linear drift that is less problematic since it can be corrected via software<sup>35,36</sup>.

In this work, we present three strategies for a MEMS gravimeter with reduced sensitivity to temperature variations  $\Delta T$ . The first one is to use materials where the thermal dependence of the expansion and that of the Young's modulus cancel each other (section III B). The second uses the expansion to exert a horizontal force along the beams, compensating the spring force variation (section III B 1). The third varies the mounting point for the sensor so that the vertical expansion moves the mass back to the original position, keeping the measurement unchanged (section III B 2). All the strate-

<sup>a)</sup> Author to whom correspondence should be addressed: egomez@ifisica.uaslp.mx

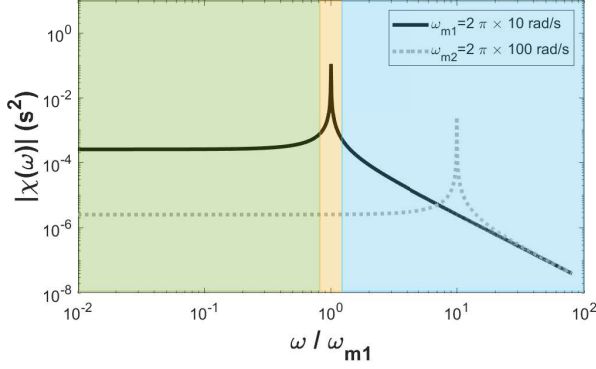


FIG. 1. The magnitude of the susceptibility  $|\chi(\omega)|$  as a function of angular frequency  $\omega$ . The solid black curve represent a gravimeter with  $\omega_{m1} = 2\pi \times 10$  rad/s and dashed gray curve with  $\omega_{m2} = 2\pi \times 100$  rad/s, both with  $Q_m = 1000$ .

gies use a DC configuration. In appendix A we analyze the fundamental sensitivity limits due to the temperature of the resonator.

## II. MECHANICAL GRAVIMETER OPERATION

Consider a mass  $m$  attached to two springs giving an effective constant  $k = k_1 + k_2$  in the vertical  $z$  direction. The mass position is described by

$$\frac{d^2 z(t)}{dt^2} + \gamma \frac{dz(t)}{dt} + \omega_m^2 z(t) = \frac{F_{ext}(t)}{m}, \quad (2)$$

with a harmonic external force  $F_{ext} = \hat{F}e^{i\omega t} = F_0 e^{i(\omega t - \delta_f)}$  and  $z = \hat{z}e^{i\omega t} = z_0 e^{i(\omega t - \delta_z)}$ , where  $F_0$  and  $z_0$  are real numbers, and  $\delta_f$  and  $\delta_z$  the phases. The solution is

$$\hat{z} = \frac{\hat{F}}{m(\omega^2 - \omega_m^2 - i\frac{\omega\omega_m}{Q_m})} = \chi(\omega)\hat{a}, \quad (3)$$

where  $\hat{a} = \hat{F}/m$  is the acceleration, and  $\chi(\omega) = (\omega^2 - \omega_m^2 - i\frac{\omega\omega_m}{Q_m})^{-1}$  is the transfer function or mechanical susceptibility, that gives the sensitivity of a DC gravimeter at  $\omega = 0$ , taking  $\hat{a} = g$  the local gravitational acceleration, Eq. (1). There are three regimes determined by  $\chi(\omega)$ . For  $\omega < \omega_m$  (green region in Fig. 1), the resonator exhibits an almost flat frequency response  $\chi \simeq 1/\omega_m^2$  and is where the DC gravimeter operates. The sensitivity is increased with a low resonant frequency  $\omega_m$  (soft spring and heavy mass). The region  $\omega \simeq \omega_m$  (narrow yellow region in Fig. 1), is where an AC gravimeter would look for a change in resonance frequency. At higher frequencies  $\omega > \omega_m$  (blue region in Fig. 1), the resonator acts as a mechanical low pass filter. Here we focus the discussion on DC gravimeters.

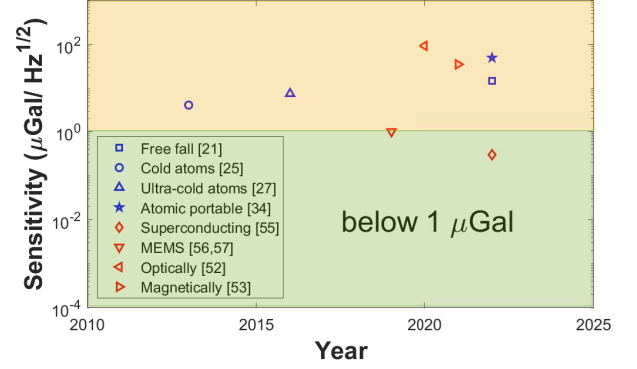


FIG. 2. Experimental sensitivities by both absolute (blue markers) and relative (red markers) gravimeters. The horizontal line indicates a sensitivity of  $1 \mu\text{Gal}/\sqrt{\text{Hz}}$ .

### A. Sensitivity, long-term stability and range

To detect the tiny variations of the local gravitational acceleration  $g$ , MEMS gravimeters must reach three goals: high sensitivity, long-term stability and wide range. Figure 2 shows the sensitivity achieved by both absolute and relative gravimeters. It includes many of the technologies available and the sensitivity that they have reached. The main limitation of MEMS gravimeters is the long-term stability, with an important contribution coming from temperature variations<sup>35,37</sup>. This includes thermal variations of the Young's modulus and the linear coefficient of thermal expansion (CTE) of silicon<sup>85</sup>, which is bigger than other materials such as fused silica used in commercial gravimeters<sup>38,86</sup>. In this work, we present three novel solutions to improve the long-term stability of MEMS gravimeter (section III B).

The range of MEMS gravimeters should be big enough to cover the variations of  $g$  on Earth due to the location, that changes from 976 Gal to 982 Gal<sup>87</sup>. It should also include the temporal variations due to Earth's tides which vary in frequency, fluctuating between diurnal ( $2 \times 10^{-5}$  Hz) and semi-diurnal ( $1 \times 10^{-5}$  Hz)<sup>35</sup>. The mass displacement is on the scale of one millimeter, something covered with current MEMS gravimeters<sup>35,37,56,57</sup>.

## III. THERMAL VARIATIONS ON THE GRAVIMETER

Thermal variations affect the measurement of  $g$  mainly through variations in the spring constant  $k$  in Eq. (1). The variation with temperature of any spatial dimension ( $z$ ) depends on the CTE ( $\alpha$ ) as

$$\frac{\Delta z}{z} = \alpha \Delta T, \quad (4)$$

and we write the change of the Young's modulus ( $E$ ) with temperature as

$$\frac{\Delta E}{E} = \alpha_E \Delta T, \quad (5)$$

where  $\alpha_E$  is the temperature coefficient of the Young's modulus.

In the section III A we study the thermal effects on  $k$  due to  $\alpha$  and  $\alpha_E$ . In section III B we propose three ways to compensate the thermal drifts to improve the long-term stability of the MEMS gravimeter.

### A. Temperature dependence of the spring constant

For the simple case of a doubly-clamped beam oscillator (bridge), the resonant frequency spectrum of a rectangular beam with uniform density  $\rho$  is described by the Euler-Bernoulli Beam Theory (EBBT) for long beams ( $L/t > 25$ ) and pure bending<sup>88,89</sup>, or by the Timoshenko Beam Theory (TBT) when the length approaches the thickness and the effect of shear and rotatory inertia is taken into account<sup>90,91</sup> (see Appendix B). The frequency spectrum of the flexural modes in the case of EBBT is given by<sup>92</sup>

$$f = \frac{\kappa_n^2 t}{4\pi\sqrt{3}L^2} \sqrt{\frac{E}{\rho}} = \frac{\kappa_n^2}{4\pi\sqrt{3}} \sqrt{\frac{E}{m}} \eta, \quad (6)$$

where  $\kappa_n = (n + \frac{1}{2})\pi$  is the eigenvalue,  $L$ ,  $t$  and  $w$  are the length, thickness and width respectively of the rectangular beam (Fig. 3), and  $\eta = \frac{t^3}{L^3}w$  is a geometric factor. When  $w \geq 25t$ , we need to replace  $E$  by  $E(1 - \nu^2)^{-1}$  in Eq. (6), as in our case. In Appendix B we show that for the MEMS gravimeter parameters and particularly for the lower modes considered, the corrections to the spectrum due to the TBT can be neglected and it is enough to use the EBBT. The spring constant using Eq. (6) is given by

$$k = m(2\pi f)^2 = \frac{\kappa_n^4}{12} \eta E. \quad (7)$$

The geometric factor  $\eta$  is temperature-dependent via  $\alpha$  in Eq. (4). As we described in the Appendix C, silicon has an isotropic behavior of  $\alpha$ , therefore

$$\frac{\Delta t}{t} = \frac{\Delta L}{L} = \frac{\Delta w}{w} = \frac{\Delta \eta}{\eta} = \alpha \Delta T. \quad (8)$$

Combining Eqs. (5), (7) and (8), we obtain

$$\begin{aligned} \frac{\Delta k}{k} &= \sqrt{\left(\frac{\Delta E}{E}\right)^2 + \left(\frac{\Delta \eta}{\eta}\right)^2} + 2\frac{\Delta E \Delta \eta}{E \eta} \\ &= (\alpha + \alpha_E) \Delta T, \end{aligned} \quad (9)$$

which shows the two thermal contributions ( $\alpha$  and  $\alpha_E$ ) to the variation of  $k$ . Taking the force as  $F = -kz$  we have

$$\Delta F = -k\Delta z - \Delta k z = F(\alpha_E + 2\alpha) \Delta T. \quad (10)$$

### B. Compensation of the effect of temperature variations

Temperature fluctuations introduce a variation in the gravimeter reading, dominated in the case of silicon by the

thermal change of the Young's modulus<sup>93</sup>, see Eq. (10). Even with a temperature control of 1 mK, there is an uncertainty contribution from thermal variations of  $25 \mu\text{Gal}$ <sup>35</sup>. The thermal sensitivity must therefore be reduced in order to reach the  $1 \mu\text{Gal}$  stability regime.

We gain some insight into the thermal sensitivity by using the analytic expression for the rectangular curved beam of Ref.<sup>94</sup>. Considering only the lowest-order term, the force right at the center of the beam is

$$F = \left(\frac{EIh}{L^3}\right) \left[\frac{3\pi^4\Theta^2}{2}\right] \Delta \left(\Delta - \frac{3}{2} + \sqrt{\frac{1}{4} - \frac{4}{3\Theta^2}}\right) \times \left(\Delta - \frac{3}{2} - \sqrt{\frac{1}{4} - \frac{4}{3\Theta^2}}\right), \quad (11)$$

with  $I = wt^3/12$  the moment of inertia of the beam and  $h$  the initial deformation of the beam (Fig. 3).  $\Delta = d/h$  is the displacement  $d$  of the central part of the beam normalized by  $h$ , and  $\Theta = h/t$ . If  $\Theta > \sqrt{16/3}$  the force changes to

$$F = \left(\frac{EIh}{L^3}\right) (8\pi^4 - 6\pi^4\Delta), \quad (12)$$

over some range of values of  $\Delta$ <sup>94</sup>.

Temperature variations have an effect on the Young's modulus and on each linear dimension ( $w$ ,  $t$ ,  $L$ ) according to Eqs. (5) and (8) (see also Appendix C and Eqs. (C4) and (C9)). If the material expansion is homogeneous, then the dimensionless quantities  $\Theta$  and  $\Delta$  do not contribute to the force variation, and all the thermal dependence is given by the term in the first parenthesis of Eqs. (11) and (12)

$$\frac{\partial F}{\partial T} = F(\alpha_E + 2\alpha), \quad (13)$$

which is the same as in Eq. (10). This is a quite general result that comes from a dimensional analysis of the force, which depends linearly on  $E$  and quadratically on a spatial dimension. In the case of silicon  $\alpha = 2.57 \times 10^{-6} \text{ K}^{-1}$ <sup>95</sup> and  $\alpha_E = -52.6 \pm 3.45 \times 10^{-6} \text{ K}^{-1}$ <sup>96</sup>, so that the effect is dominated by  $\alpha_E$ .

Fabricating the sensor not with silicon, but with a material with  $\alpha_E = -2\alpha$  should remove the dependence of the force on the temperature, that is, the effect of the change in Young's modulus would be canceled by the linear expansion. Table I gives a list of alloys made out of two materials that meet the above condition. Their properties change rapidly around a particular percentage of the second material. The second column gives the percentages that fulfill the above condition, where the first value we quote on each one has a less abrupt dependence on percentage, making it the more robust choice. Beams fabricated with the materials listed in Table 1, would give a bending behavior that remains constant with varying temperature, a quite interesting property for many applications. The problem is the availability of such alloys and the fact that they are not compatible with the same fabrication techniques as silicon, which is the material of choice for MEMS devices. In what follows we present two alternative

TABLE I. Alloys that fulfil the condition  $\alpha_E = -2\alpha$  at a particular percentage of the second material. In the second column, the first percentage value would be the more robust one.

Material	Percentage for $\alpha_E = -2\alpha$	$\alpha$ ( $10^{-6}$ )
Cobalt-Palladium <sup>97</sup>	90, 96	-32.4
Iron-Palladium <sup>98</sup>	78, 51	-15
Nickel-Copper <sup>99</sup>	29, 30.5	-29
Iron-Platinum <sup>100</sup>	70, 51	-17
Nickel-Palladium <sup>101</sup>	88, 46, 59.5, 73	16.4
Nickel-Platinum <sup>101</sup>	50, 61	12.6

mechanisms that can be used to enhance the effect of the linear expansion to cancel the variation due to the Young's modulus, which work with silicon and do not require any special materials. The first one takes advantage of an additional longitudinal force induced in the beam due to the expansion. The second one changes the mounting point for the frame of the sensor, to obtain a displacement of the slit with temperature, given that the gravimetry measurement relies on determining the slit position.

### 1. Force from the longitudinal expansion

High sensitivity on a MEMS gravimeter is achieved by having a weak spring constant  $k$  around the operation point. This is achieved by combining two different springs with positive and negative stiffness respectively<sup>37</sup>. We can use Eqs. (11) and (12) to quantify the effect of both. Consider the test mass supported by two curved beams as shown in Fig. 3. The upper beam is designed to have negative stiffness at the operating point, whereas the lower one has positive stiffness. We consider beams of the same width ( $w$ ) since they would be fabricated from a single silicon wafer. By carefully adjusting the parameters of the beams, which are different for the upper and lower beam, one can obtain a total force at the operating point (where  $F = mg$ ) with a slope close to zero, that is, with a weak spring constant ( $k = 1$  N/m). We consider a test mass of  $m = 0.3$  g.

Applying an axial external force ( $F_e$ ) on the lower beam that is described by Eq. (11), modifies the force to

$$F = \left( \frac{Elh}{L^3} \right) \left[ \frac{3\pi^4\Theta^2}{2} \Delta \left( \Delta - \frac{3}{2} + \sqrt{\frac{1}{4} - \frac{4}{3\Theta^2}} \right) \times \left( \Delta - \frac{3}{2} - \sqrt{\frac{1}{4} - \frac{4}{3\Theta^2}} \right) + \frac{\pi^2 L^2}{2EI} (1 - \Delta) F_e \right] \quad (14)$$

We want to use this force to compensate the variation of the gravimeter reading due to temperature fluctuations. To do this, suppose we add a piece of a rigid material with no thermal expansion (for example, Ultra Low Expansion (ULE) material) parallel to the beam, as shown in Fig. 3. On one side both pieces are attached to a fixed common surface, while on the other there is a cantilever fixed to the ULE material that is barely touching the gravimeter. At the operating temper-

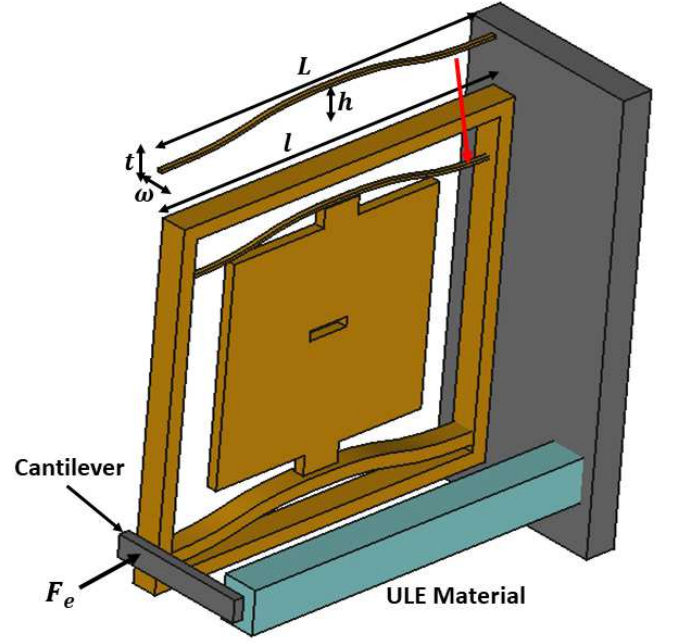


FIG. 3. MEMS gravimeter (brown) with longitudinal force mechanism for temperature compensation. The blue bar is made out of a Ultra Low Expansion (ULE) material. The gravimeter and the bar are both attached to a common surface. The parameters of the beams are shown on top.

ature, the cantilever exerts no force, but as the temperature increases, the beam expands by  $\Delta l = l\alpha\Delta T$  while the ULE material maintains a constant length, so that the cantilever exerts an axial force ( $F_e$  in Eq. (14)) on the beam given by

$$F_e = \kappa\Delta l = \kappa l\alpha\Delta T, \quad (15)$$

with  $\kappa$  the spring constant associated with the cantilever action, and  $l \simeq L$  the size of the gravimeter silicon piece, assuming a thin gravimeter frame. The ULE material works as a reference length that does not expand with temperature, so that the force introduced by the cantilever depends only on the expansion of the MEMS gravimeter itself.

Consider the slit at a particular position ( $d_0$ ) and temperature ( $T_0$ ). With a small temperature change and displacement of the slit, the force in Eq. (14) changes to

$$F = F + \frac{\partial F}{\partial d}\Delta d + \frac{\partial F}{\partial T}\Delta T, \quad (16)$$

with  $\Delta d = (d - d_0)$ , and equating the force to the test mass weight gives the slit displacement

$$\Delta d = -\frac{(\partial F/\partial T)}{(\partial F/\partial d)}\Delta T. \quad (17)$$

There are now two contributions to the temperature dependence

$$\frac{\partial F}{\partial T} = \left[ F(\alpha_E + 2\alpha) + \frac{\pi^2}{2}\alpha h_2 \kappa_2 (1 - \Delta_2) \right], \quad (18)$$



the first term corresponds to the one given by Eq. (13), and the second one is related with the force from Eq. (15) on the lower (positive stiffness) beam. The operating point on a gravimeter for the negative stiffness beam has a displacement close to  $\Delta_1 = 1$ . Since the effect of the force scales as  $(1 - \Delta)$  as in Eq. (18), it is more effective to apply the force in the positive stiffness beam. This contribution can be made positive or negative depending on the sign of  $h_2$ , that is, on the direction of the prefabricated deformation. When the temperature increases, the force is reduced as in Eq. (13) because  $\alpha_E$  is negative, and the slit position gets lowered under the action of gravity. To compensate this change, the extra term must exert a positive (upwards) force, which amounts to have a positive  $h_2$ .

The temperature dependence is cancelled by setting the square parenthesis in Eq. (18) to zero, that is, by having a spring constant of the cantilever equal to

$$\kappa_2 = -\frac{2F(\alpha_E + 2\alpha)}{\pi^2 \alpha h_2 (1 - \Delta_2)}. \quad (19)$$

A typical (silicon) beam would end up requiring a  $\kappa_2$  around 100 N/m, which is about the same as that of an aluminum cantilever of length of 1 cm, width of 1 mm and thickness of 0.2 mm.

The application of an axial force with a V-beam actuator can be used to tune the stiffness of the beams in the gravimeter<sup>84</sup>. The authors in that reference proposed measuring the temperature in a feedback loop to the actuator to correct for the temperature dependence. The compensation proposed in Eq. (19) has the advantage that the correction does not depend on the quality of the feedback loop, since the change in temperature of the sensor introduces the beam expansion that corrects automatically the variation in the force.

## 2. Compensation through an expansion

Another option to correct for the temperature dependence is to apply the correction not in the force, but in the displacement of the slit in the sensor. The variation in the force introduces a slit displacement given by Eq. (17). Taking an anchoring point for the sensor displaced vertically by a distance  $L_p$  with respect to the slit, produces a slit displacement due to the thermal expansion of the sensor of  $\Delta L_p = L_p \alpha \Delta T$  according to Eq. (4). The position of the slit remains unchanged with temperature variations if  $\Delta d = \Delta L_p$ , that is

$$L_p = -\frac{F}{k} \left( \frac{\alpha_E + 2\alpha}{\alpha} \right), \quad (20)$$

with  $k$  the spring constant of the sensor and  $F = mg$ . For our parameters we obtain  $L_p = 5.4$  cm. Figure 4 shows a more detailed drawing of the proposed configuration. The slit, the LED and quadrant detector they all lie at the same height. A bar of a non expanding material (ULE for example) is mounted at that same height, while the sensor frame is attached at the opposite end of the ULE material of length  $L_p$ . The height of this holding point ( $P$ ) for the sensor would not

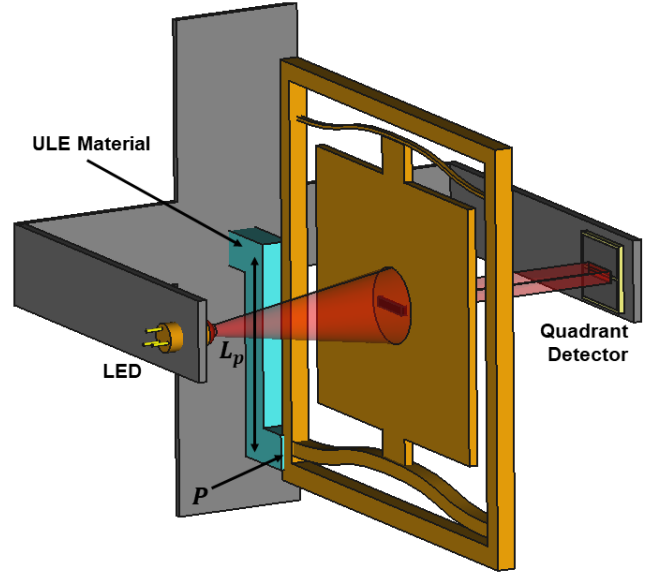


FIG. 4. MEMS gravimeter (brown) with slit displacement mechanism for temperature compensation. The blue bar is made out of a Ultra Low Expansion material. The attachment point ( $P$ ) for the sensor is at a distance  $L_p$  lower compared to the height of the slit.

be affected by a temperature change due to the use of an ULE material. Both slit displacements ( $\Delta d$  and  $\Delta L_p$ ) are generated by the same temperature change ( $\Delta T$ ), which depends only on the temperature of the sensor itself. The sensor is small and has good thermal conductivity ( $148 \text{ WK}^{-1} \text{m}^{-1}$ <sup>102,103</sup>), ensuring a uniform temperature throughout the sensor, and therefore a robust cancellation mechanism. Fine tuning of the correction is achieved by changing the attachment distance  $L_p$ .

One can reduce  $L_p$  in order to keep a small detector by increasing  $k$ , at the expense of having less sensitivity to gravity. In other words, there would be a trade off between having more sensitivity and having temperature insensitivity. Increasing  $k$  by a factor of 2, gives an  $L_p$  two times smaller, at the price of having to integrate 4 times more to reach the same precision. Fortunately, as we show in Section II A, these sensors have shown very good sensitivity<sup>37</sup>, making it worth while to sacrifice some of this sensitivity for stability. We emphasize that the two compensation mechanisms that we propose depend only on the sensor's temperature, made out of a single piece of silicon, rather than on the temperature of two different pieces, making them robust compensation mechanisms. Assembling the cantilever for the second strategy might be quite challenging, but implementing the third strategy seems within reach and requires carefully gluing the components at the right height. The thermal expansion of the ULE material must be small compared to that of silicon, the material of the sensor. This is the case working within a few degrees of the optimum temperature of the ULE material.

#### IV. CONCLUSIONS

Temperature variations cause the main limitation for the long-term stability of MEMS gravimeters. They affect the spring constant because of two reasons: due to the thermal expansion that changes the dimensions of a particular design, and from a thermal variation in the Young's modulus. We propose three methods to reduce the temperature sensitivity. It is suppressed for materials that fulfill the condition  $\alpha_E = -2\alpha$ , that is, that the thermal expansion is canceled by the thermal variation of the Young's modulus. We present several materials that meet this condition, reducing the sensitivity to temperature variations. MEMS gravimeters are usually made out of crystalline silicon, making it hard to use this previous strategy. An alternative is to use the sensor's own thermal expansion to introduce a force that cancels the variation in the spring constant due to temperature. Finally, we present a third alternative that focus on the displacement of the mass, which is what the sensor measures, rather than on the force. Adjusting the anchoring point of the sensor, it is possible to introduce a thermal expansion that compensates for the proof mass displacement due to the change in the spring constant. All these proposals are robust compensation mechanisms since they only depend on the temperature of the sensor itself.

#### ACKNOWLEDGMENTS

We wish to acknowledge the financial support of COPOCYT Trust 23871, CONACYT A1-S-18696, CF G40 and PROFAPI PRO-A1-004 (UAS).

#### DATA AVAILABILITY STATEMENT

The data that support the findings of this study are available from the corresponding author upon reasonable request.

#### Appendix A: Temperature variations from mechanical noise

In this Appendix we analyze the sensitivity limits due to the temperature of the resonator, and the temperature variation  $\Delta T$  due to different mechanical noise sources. We ignore the dissipation channels and assume that all that energy is converted into heat. This determines how big the quality factor  $Q_m$  must be.

Thermomechanical noise gives a sensitivity limit for MEMS gravimeters in thermal equilibrium. Applying a stochastic force to the harmonic oscillator model described in section II, results in a Brownian motion, which generates the thermomechanical displacement noise. The Nyquist theorem gives the thermal noise generated by a system in thermal equilibrium. In analogy with electricity, the thermomechanical force noise is<sup>104</sup>

$$\langle F^2 \rangle = 4k_B T \frac{m\omega_m}{Q_m} B, \quad (\text{A1})$$

where  $k_B$  is the Boltzmann constant, and  $B$  is the bandwidth. The thermomechanical acceleration noise is

$$\langle a_{th} \rangle = \sqrt{\frac{\langle F^2 \rangle}{m^2}} = \sqrt{4k_B T \frac{\omega_m}{mQ_m} B}. \quad (\text{A2})$$

In the case of MEMS gravimeters based on a quasi-zero stiffness design, the theoretical acceleration noise floor at room temperature goes from  $0.5 \mu\text{Gal}/\sqrt{\text{Hz}^{35}}$  up to  $0.08 \mu\text{Gal}/\sqrt{\text{Hz}^{37}}$ , which shows that sensitivity is not a limitation for a MEMS gravimeter. The last formula indicates that low frequency and high mechanical quality factors are always preferred. A DC gravimeter<sup>37</sup> reaches a sensitivity of about  $1 \mu\text{Gal}$  with  $Q_m > 200$ , which is not too demanding.

We now calculate the temperature variations  $\Delta T$  due to mechanical noise sources. The power can be written as

$$P = \frac{d}{dt}(K + U) + \gamma m \left( \frac{dz}{dt} \right)^2, \quad (\text{A3})$$

where  $K = \frac{1}{2}m(dz/dt)^2$  and  $U = \frac{1}{2}m\omega_m^2 z^2$  are the kinetic and the potential energy, respectively (the energy stored in the oscillation) and the last term gives the dissipation. Assuming a sinusoidal driven force  $F_{ext} = F_0 \cos(\omega t)$ , the general solution is  $z(t) = z_0 \cos(\omega t + \delta_z)$  where  $z_0 = \frac{F_0/m}{\sqrt{(\omega_m^2 - \omega^2)^2 + (\omega_m \omega / Q_m)^2}}$  (3) and  $\delta_z = \arctan\left(\frac{\omega_m^2 - \omega^2}{\omega_m \omega / Q_m}\right) - \frac{\pi}{2}$ . In steady state  $\frac{d}{dt}\langle K + U \rangle = 0$ , and the last term in Eq. (A3) gives the energy that is dissipated into heat

$$\langle P \rangle = \left\langle \gamma m \left( \frac{dz}{dt} \right)^2 \right\rangle = \frac{1}{2} m \frac{\omega_m \omega^2}{Q_m} z_0^2, \quad (\text{A4})$$

The temperature change  $\Delta T$  per unit time  $\Delta t$  is

$$\frac{\Delta T}{\Delta t} = \frac{\langle P \rangle}{mc(T)} = \frac{1}{2c(T)} \frac{\omega_m \omega^2}{Q_m} z_0^2, \quad (\text{A5})$$

with  $c(T)$  the specific heat capacity.

Under real conditions, some of the dominant mechanical noise sources may be due to acoustic, building motion or rail-road noise. The acoustic noise corresponds to the dominant contribution, giving a heating rate below  $5 \times 10^{-4} \text{ K/s}$  taking silicon ( $c(T) = 710 \text{ J/kg} \cdot \text{K}$  at a pressure of  $1 \text{ Pa}^{105}$ ) with a conservative mechanical quality factor of 1200 and a fundamental vibration frequency of  $3 \text{ Hz}^{37}$ . A temperature stabilization of about  $1 \text{ mK}$  should be enough to overcome most of the above heating mechanisms.

#### Appendix B: Timoshenko Beam Theory

The EBBT of flexural motion has been known to be inadequate for higher modes or when the effect of the cross-sectional dimensions cannot be neglected. For those cases, the TBT includes the effect of rotatory inertia and transverse-shear deformation. The coupled equations are<sup>106</sup>

$$EI \frac{\partial^2 \phi}{\partial x^2} - KAG \left( \frac{\partial v}{\partial x} + \phi \right) - \rho I \frac{\partial^2 \phi}{\partial t^2} = 0, \quad (\text{B1})$$

$$KAG \left( \frac{\partial^2 v}{\partial x^2} + \frac{\partial \phi}{\partial x} \right) - \rho A \frac{\partial^2 v}{\partial t^2} = 0, \quad (\text{B2})$$

with  $G$  and  $E$  the shear and Young's modulus,  $K$ ,  $A$  and  $I$  the shear coefficient, area, and moment of inertia of the beam cross-section respectively,  $v$  the transversal displacement and  $\phi$  the cross-section rotation. Combining Eqs. (B1) and (B2) gives<sup>107</sup>

$$EI \frac{\partial^2 v}{\partial x^4} - \rho I \left( 1 + \frac{E}{KG} \right) \frac{\partial^4 v}{\partial x^2 \partial t^2} + \rho A \frac{\partial^2 v}{\partial t^2} + \frac{\rho^2 I}{KG} \frac{\partial^2 v}{\partial t^4} = 0. \quad (\text{B3})$$

Similarly, an equation for  $\phi$  can be obtained.

Writing

$$v(x, t) = V(x)e^{i\omega t}, \quad \phi(x, t) = \Phi(x)e^{i\omega t}, \quad (\text{B4})$$

gives

$$\begin{aligned} \frac{\partial^4 V}{\partial x^4} + \frac{\rho \omega^2}{E} \left( 1 + \frac{E}{KG} \right) \frac{\partial^2 V}{\partial x^2} + \\ \frac{\rho \omega^2}{E} \left( \frac{\rho \omega^2}{KG} - \frac{A}{I} \right) V = 0. \end{aligned} \quad (\text{B5})$$

The solutions has the form  $V(x) = e^{\lambda^* x}$  with

$$\begin{aligned} \lambda_+^{*2}, \lambda_-^{*2} = & -\frac{\rho \omega^2}{2E} \left( 1 + \frac{E}{KG} \right) \\ & \pm \sqrt{\frac{\rho^2 \omega^4}{4E^2} \left( 1 - \frac{E}{KG} \right)^2 + \frac{\rho \omega^2 A}{EI}}, \end{aligned} \quad (\text{B6})$$

which is related to the resonant frequencies for a given particular beam shape and boundary condition. In particular for a rectangular cross-section and a doubly-clamped beam, we have  $K = \frac{2(1+\nu)}{4+3\nu}$ <sup>108</sup>,  $\frac{I}{A} = \frac{t^2}{12}$  and  $G = \frac{E}{2(1+\nu)}$ <sup>109</sup>. The frequency analysis is divided into two cases with respect to the *transition frequency*  $\tilde{\omega}^2 = \frac{KGA}{\rho I}$ , which is the value where  $\lambda_+^{*2}$  changes from positive to negative ( $\lambda_-^{*2}$  is always negative).

For the existence of non-trivial solutions, the following transcendental equation must be satisfied

$$2(1 - \cosh(\lambda_1 L) \cos(\lambda_2 L)) \pm \frac{\lambda_1 \lambda_2}{\alpha_1 \alpha_2} \left( \frac{\alpha_2^2}{\lambda_2^2} \mp \frac{\alpha_1^2}{\lambda_1^2} \right) \sinh(\lambda_1 L) \sin(\lambda_2 L) = 0, \quad (\text{B7})$$

where the upper and lower signs are for  $\omega^2 < \tilde{\omega}^2$  and  $\omega^2 > \tilde{\omega}^2$  respectively, and we have the real numbers

$$\begin{aligned} \lambda_1 = & \begin{cases} +\sqrt{+\lambda_1^{*2}} > 0 & \text{for } \omega^2 < \tilde{\omega}^2 \\ +\sqrt{-\lambda_1^{*2}} > 0 & \text{for } \omega^2 > \tilde{\omega}^2 \end{cases} \\ \lambda_2 = & +\sqrt{-\lambda_2^{*2}} > 0 \end{aligned} \quad (\text{B8})$$

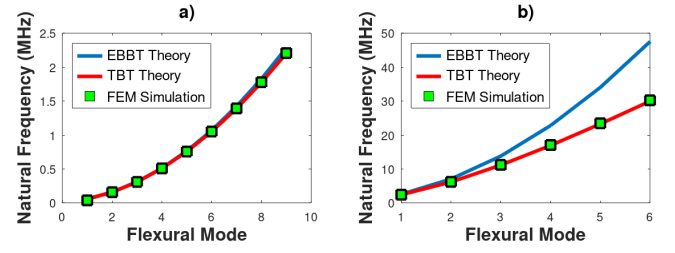


FIG. 5. Natural frequencies of a doubly-clamped beam from the EBBT (solid blue), TBT (solid red) and finite element simulations (FEM, green square markers) for an aspect ratio of a)  $L/t = 10$  and b)  $L/t = 66$ .

TABLE II. Room temperature properties of single crystalline silicon (100).

Property	Value
Density <sup>111</sup>	2330 kg/m <sup>3</sup>
Young's modulus <sup>112,113</sup>	$130 \times 10^9$ Pa
Thermal conductivity <sup>102,103</sup>	148 W/(m · K)
Poisson ratio <sup>112</sup>	0.28
CTE <sup>114,115</sup>	$2.56 \times 10^{-6}$ 1/K
Specific heat capacity <sup>116</sup>	702 J/(kg · K)

and

$$\begin{aligned} \alpha_1 = & \begin{cases} \frac{\rho \omega^2}{KG} + \lambda_1^2 & \text{for } \omega^2 < \tilde{\omega}^2, \\ \frac{\rho \omega^2}{KG} - \lambda_1^2 & \text{for } \omega^2 > \tilde{\omega}^2, \end{cases} \\ \alpha_2 = & \frac{\rho \omega^2}{KG} - \lambda_2^2. \end{aligned} \quad (\text{B9})$$

Figure 5 shows that for high aspect ratios, the EBBT and TBT almost gives the same result for the lower vibration modes. For small aspect ratios, EBBT and TBT start to deviate from each other, but EBBT still gives a similar result to TBT and the finite element simulations (FEM) for the fundamental mode with deviations below 1%.

### Appendix C: Temperature dependence of silicon properties

We consider the use of single crystalline silicon (100) for the MEMS gravimeter. Table II lists some of its properties at room temperature. The variations of the CTE and Young's modulus with temperature have been extensively studied for crystalline silicon<sup>110</sup>. In this Appendix we model the dependence of  $\alpha$  and  $\alpha_E$  with temperature.

#### 1. Linear coefficient of thermal expansion, $\alpha$

The linear coefficient of thermal expansion  $\alpha$ , at some temperature  $T$ , is defined as the change in length  $L(T)$  with respect to the length  $L_0$  at some fixed temperature  $T_0$ , usually

taken as the room temperature  $T_0 = 293.15 \text{ K}$ <sup>117</sup>

$$\alpha = \frac{d(\ln L)}{dT} \approx \frac{1}{L_0} \frac{dL}{dT}. \quad (\text{C1})$$

The approximate Eq. (4) works very well because usually  $L/L_0 - 1$  is very small for all temperatures. In all cubic crystals  $\alpha$  is a scalar, independent of the direction<sup>95,117</sup>. In single-crystal silicon a 5<sup>th</sup> order polynomial (dashed gray line in Fig. 6) gives a good fit to the experimental data (hollow red diamonds) in the range from 293 K to 1000 K<sup>95,118</sup>, that is

$$\frac{\alpha(T)}{10^{-6} \text{ K}^{-1}} = a_0 + a_1 T + a_2 T^2 + a_3 T^3 + a_4 T^4 + a_5 T^5, \quad (\text{C2})$$

where  $a_0 = -3.0451$ ,  $a_1 = 0.035705$ ,  $a_2 = -7.981 \times 10^{-5}$ ,  $a_3 = 9.5783 \times 10^{-8}$ ,  $a_4 = -5.8919 \times 10^{-11}$  and  $a_5 = 1.4614 \times 10^{-14}$ . This fit does not work well for  $T \leq T_0$ . A good fit to the data in range from 0 K to 600 K (hollow green squares in Fig. 6) is given by a more complicated expression for (solid black line)<sup>119–122</sup>:

$$\begin{aligned} \frac{\alpha(T)}{10^{-6} \text{ K}^{-1}} = & \left( b_0 T^3 + (b_1 T^5 + b_2 T^{5.5} + b_3 T^6 + b_4 T^{6.5} + b_5 T^7) \left( \frac{1 + \text{erf}(T_1)}{2} \right) \right) \left( \frac{1 - \text{erf}(0.2T_2)}{2} \right) \\ & + \left( (-b_6 + b_7 T_3^2 + b_8 T_3^3 + b_9 T_3^9) \left( \frac{1 + \text{erf}(0.2T_2)}{2} \right) \right) \left( \frac{1 - \text{erf}(0.1T_4)}{2} \right) \\ & + \left( b_{10} + \frac{b_{11}}{T} + \frac{b_{12}}{T^2} + \frac{b_{13}}{T^3} \right) \left( \frac{1 + \text{erf}(0.1T_4)}{2} \right), \end{aligned} \quad (\text{C3})$$

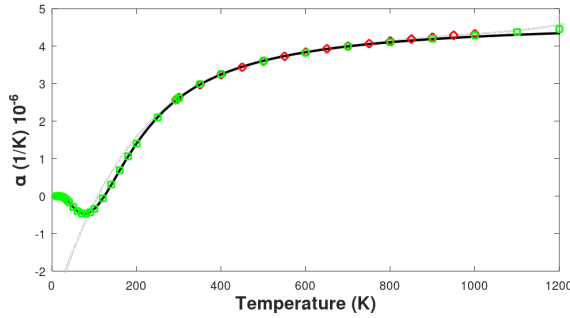


FIG. 6. Compilation of experimental data taken by other groups for  $\alpha(T)$  for  $T > T_0$  (hollow red diamonds) fitted by Eq. (C2) (dashed gray line)<sup>95</sup>, and for the full temperature range (hollow green squares)<sup>120</sup> fitted by Eq. (C3) (black solid line)<sup>119,122</sup>.

where  $b_0 = 4.8 \times 10^{-5}$ ,  $b_1 = 1.00500 \times 10^{-5}$ ,  $b_2 = -5.99688 \times 10^{-6}$ ,  $b_3 = 1.25574 \times 10^{-6}$ ,  $b_4 = -1.12086 \times 10^{-7}$ ,  $b_5 = 3.63225 \times 10^{-9}$ ,  $b_6 = -47.6$ ,  $b_7 = 2.67708 \times 10^{-2}$ ,  $b_8 = -1.22829 \times 10^{-4}$ ,  $b_9 = 1.62544 \times 10^{-18}$ ,  $b_{10} = 4.72374 \times 10^2$ ,  $b_{11} = -3.58796 \times 10^4$ ,  $b_{12} = -1.24191 \times 10^7$ ,  $b_{13} = 1.25972 \times 10^9$ ,  $T_1 = T - 15$ ,  $T_2 = T - 52$ ,  $T_3 = T - 76$  and  $T_4 = T - 200$ .

For small variations around room temperature  $T_0$  a linear approximation is good enough

$$\alpha(T) = \alpha_0 + 2\alpha_1(T - T_0), \quad (\text{C4})$$

with  $\alpha_0 = 2.5554 \times 10^{-6} \text{ K}^{-1}$  and  $\alpha_1 = 4.58 \times 10^{-9} \text{ K}^{-2}$  (Fig. 7). This approximation has been verified experimentally from

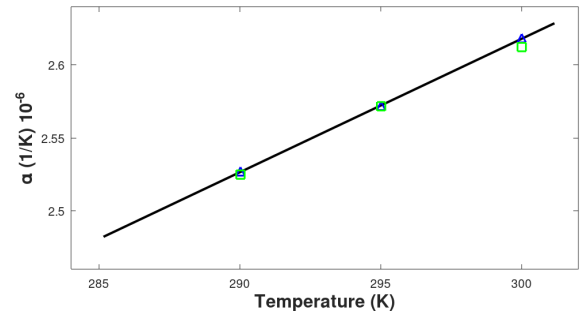


FIG. 7. Compilation of experimental data taken by other groups for  $\alpha(T)$  around  $T_0$ <sup>123,125</sup> and linear fit by Eq. (C4).

285.15 K to 301.15 K<sup>115,123–125</sup> (hollow blue triangles and hollow green squares in Fig. 7). The deviation from linearity gives a relative error on  $\alpha$  of around 10 ppm<sup>123</sup>.

## 2. Young's modulus temperature coefficient $\alpha_E$

When an isotropic solid beam of length  $L$  is loaded in pure tension, the tensile stress vector is given by  $\sigma$  and the longitudinal strain vector is approximately  $\epsilon \sim \Delta L/L$ , with  $\Delta L$  the length increase. Hooke's Law states that<sup>114</sup>

$$\epsilon = s\sigma, \quad (\text{C5})$$

where  $s = 1/c$  is the elastic compliance constant and  $c$  the elastic stiffness constant or Young's modulus  $E$ .



The compliance  $s_{ij}$  with  $\{i, j\} = 1, 2, \dots, 6$  is a matrix. For anisotropic materials possessing a cubic crystal structure such as silicon, the matrix  $s_{ij}$  contains three independent elastic constants,  $s_{11}$ ,  $s_{12}$  and  $s_{44}$  from which the Young's modulus in any crystal direction  $[hkl]$  can be calculated as

$$\frac{1}{E_{hkl}} = s'_{11} = s_{11} - 2 \left( s_{11} - s_{12} - \frac{1}{2}s_{44} \right) \times (l_1^2 l_2^2 + l_2^2 l_3^2 + l_3^2 l_1^2), \quad (C6)$$

where  $l_i$  are the direction cosines along the axis<sup>126,127</sup>. Usually, experimental data is given for  $c_{ij}$ , instead  $s_{ij}$ , and their relations for silicon are

$$c_{11} = \frac{s_{11} + s_{12}}{(s_{11} - s_{12})(s_{11} + 2s_{12})}, \quad c_{12} = \frac{-s_{12}}{(s_{11} - s_{12})(s_{11} + 2s_{12})}, \quad c_{44} = \frac{1}{s_{44}}. \quad (C7)$$

Using  $c_{11} = 165.5$  GPa,  $c_{12} = 63.9$  GPa and  $c_{44} = 79.5$  GPa for silicon at room temperature<sup>127</sup>, we get  $s_{11} = 7.68 \times 10^{-12} \text{ Pa}^{-1}$ ,  $s_{12} = -2.14 \times 10^{-12} \text{ Pa}^{-1}$  and  $s_{44} = 12.6 \times 10^{-12} \text{ Pa}^{-1}$ <sup>128</sup>.

For a particular tension direction,  $E$  is defined as the ratio of the longitudinal stress to the longitudinal strain, that is,  $E_{hkl} = 1/s'_{11}$ . For the case of tension applied in the  $[100]$  direction, we have  $l_1 = \cos(0) = 1$ ,  $l_2 = \cos(\pi/2) = 0$  and  $l_3 = \cos(\pi/2) = 0$ , then  $E_{100} = 1/s_{11} = 130 \text{ GPa}$ <sup>113</sup>, the minimum value for silicon. For the  $[110]$  direction, i.e., the direction parallel to the major flat of a (100) wafer, the cosines are  $l_1 = \cos(\pi/2) = 0$ ,  $l_2 = \cos(\pi/4) = 1/\sqrt{2}$ ,  $l_3 = \cos(3\pi/4) = -1/\sqrt{2}$ , then  $E_{110} = 169 \text{ GPa}$ <sup>113</sup>.

The temperature dependence of the Young's modulus ( $\alpha_E$ ) should be given by the thermoelastic theory, but it is hard to obtain from a simple model over a wide temperature range. However, it possible to use a semi-empirical formula<sup>129</sup>

$$E(T) = E_{T=0} - BT \exp\left(-\frac{T_r}{T}\right), \quad (C8)$$

with  $E_{T=0}$  the value of Young's modulus at absolute zero temperature, and  $T_r > 0$  (related to the Debye temperature) and  $B > 0$  two constants. Their values for silicon are obtained experimentally to be  $E_{T=0} = 167.5$  GPa,  $T_r = 317$  K and  $B = 15.8 \text{ MPa/K}$ <sup>96</sup>.

Using (5) and (C8), we have

$$\alpha_E(T) = \frac{1 + \frac{T_r}{T}}{T - \frac{E_{T=0}}{B} \exp\left(-\frac{T_r}{T}\right)}. \quad (C9)$$

The variation of  $E(T)$  around room temperature is very linear, giving an almost constant  $\alpha_E$ , with an average value for silicon in the temperature range 200 – 300 K of  $\alpha_E = -52.6 \text{ ppm/K}$ <sup>96</sup>.

## REFERENCES

- <sup>1</sup>G. M. Tino, "Testing gravity with cold atom interferometry: results and prospects," *Quantum Science and Technology* **6**, 024014 (2021).
- <sup>2</sup>D. C. Moore and A. A. Geraci, "Searching for new physics using optically levitated sensors," *Quantum Science and Technology* **6**, 014008 (2021).
- <sup>3</sup>T. Westphal, H. Hepach, J. Pfaff, and M. Aspelmeyer, "Measurement of gravitational coupling between millimetre-sized masses," *Nature* **591**, 225–228 (2021).
- <sup>4</sup>G. Amelino-Camelia, "Gravity in quantum mechanics," *Nature Physics* **10**, 254–255 (2014).
- <sup>5</sup>M. Arndt and K. Hornberger, "Testing the limits of quantum mechanical superpositions," *Nature Physics* **10**, 271–277 (2014).
- <sup>6</sup>D. Carney, P. C. E. Stamp, and J. M. Taylor, "Tabletop experiments for quantum gravity: a user's manual," *Classical and Quantum Gravity* **36**, 034001 (2019).
- <sup>7</sup>D. Carney, S. Ghosh, G. Krnjaic, and J. M. Taylor, "Proposal for gravitational direct detection of dark matter," *Phys. Rev. D* **102**, 072003 (2020).
- <sup>8</sup>D. Carney, G. Krnjaic, D. C. Moore, C. A. Regal, G. Afek, S. Bhawe, B. Brubaker, T. Corbitt, J. Cripe, N. Crisosto, A. Geraci, S. Ghosh, J. G. E. Harris, A. Hook, E. W. Kolb, J. Kunjummen, R. F. Lang, T. Li, T. Lin, Z. Liu, J. Lykken, L. Magrini, J. Manley, N. Matsumoto, A. Monte, F. Monteiro, T. Purdy, C. J. Riedel, R. Singh, S. Singh, K. Sinha, J. M. Taylor, J. Qin, D. J. Wilson, and Y. Zhao, "Mechanical quantum sensing in the search for dark matter," *Quantum Science and Technology* **6**, 024002 (2021).
- <sup>9</sup>N. Yazdi, F. Ayazi, and K. Najafi, "Micromachined inertial sensors," *Proceedings of the IEEE* **86**, 1640–1659 (1998).
- <sup>10</sup>D. K. Shaeffer, "Mems inertial sensors: A tutorial overview," *IEEE Communications Magazine* **51**, 100–109 (2013).
- <sup>11</sup>F. Greco, G. Currenti, G. D'Agostino, A. Germak, R. Napoli, A. Pistorio, and C. Del Negro, "Combining relative and absolute gravity measurements to enhance volcano monitoring," *Bulletin of Volcanology* **74**, 1745–1756 (2012).
- <sup>12</sup>D. Carbone, M. P. Poland, M. Diamant, and F. Greco, "The added value of time-variable microgravimetry to the understanding of how volcanoes work," *Earth-Science Reviews* **169**, 146–179 (2017).
- <sup>13</sup>Y. Imanishi, T. Sato, T. Higashi, W. Sun, and S. Okubo, "A network of superconducting gravimeters detects submicrorogal coseismic gravity changes," *Science* **306**, 476–478 (2004).
- <sup>14</sup>X. Zou, P. Thiruvengatanathan, and A. A. Seshia, "A seismic-grade resonant mems accelerometer," *Journal of Microelectromechanical Systems* **23**, 768–770 (2014).
- <sup>15</sup>J.-P. Montagner, K. Juhel, M. Barsuglia, J. P. Ampuero, E. Chassande-Mottin, J. Harms, B. Whiting, P. Bernard, E. Clévédy, and P. Lognonné, "Prompt gravity signal induced by the 2011 Tohoku-Oki earthquake," *Nature Communications* **7**, 13349 (2016).
- <sup>16</sup>T. Jacob, R. Bayer, J. Chery, and N. Le Moigne, "Time-lapse micro-gravity surveys reveal water storage heterogeneity of a karst aquifer," *Journal of Geophysical Research: Solid Earth* **115** (2010), <https://doi.org/10.1029/2009JB006910>.
- <sup>17</sup>M. Van Camp, O. de Viron, A. Watlet, B. Meurers, O. Francis, and C. Caudron, "Geophysics from terrestrial time-variable gravity measurements," *Reviews of Geophysics* **55**, 938–992 (2017).
- <sup>18</sup>Q. Chaffaut, N. Lesparre, F. Masson, J. Hinderer, D. Viville, J.-D. Bernard, G. Ferhat, and S. Cotel, "Hybrid gravimetry to map water storage dynamics in a mountain catchment," *Frontiers in Water* **3** (2022), 10.3389/frwa.2021.715298.
- <sup>19</sup>T. van Dam, O. Francis, J. Wahr, S. Khan, M. Bevis, and M. van den Broeke, "Using gps and absolute gravity observations to separate the effects of present-day and pleistocene ice-mass changes in south east greenland," *Earth and Planetary Science Letters* **459**, 127–135 (2017).
- <sup>20</sup>S.-Y. Wang, J. L. Chen, C. R. Wilson, J. Li, and X. Hu, "Reconciling GRACE and GPS estimates of long-term load deformation in southern Greenland," *Geophysical Journal International* **212**, 1302–1313 (2017).
- <sup>21</sup><https://microglacoste.com>, "Micro-g lacoste, fg5-x absolute gravimeter," (2022).
- <sup>22</sup>M. Kasevich and S. Chu, "Atomic interferometry using stimulated raman transitions," *Phys. Rev. Lett.* **67**, 181–184 (1991).
- <sup>23</sup>A. Peters, K. Y. Chung, and S. Chu, "Measurement of gravitational acceleration by dropping atoms," *Nature* **400**, 849–852 (1999).
- <sup>24</sup>K. Bongs, M. Holynski, J. Vovrosh, P. Bouyer, G. Condon, E. Rasel, C. Schubert, W. P. Schleich, and A. Roura, "Taking atom interferometric quantum sensors from the laboratory to real-world applications," *Nature Reviews Physics* **1**, 731–739 (2019).

- <sup>25</sup>Z.-K. Hu, B.-L. Sun, X.-C. Duan, M.-K. Zhou, L.-L. Chen, S. Zhan, Q.-Z. Zhang, and J. Luo, "Demonstration of an ultrahigh-sensitivity atom-interferometry absolute gravimeter," *Phys. Rev. A* **88**, 043610 (2013).
- <sup>26</sup>D. Aguilera, H. Ahlers, B. Battelier, A. Bawamia, A. Bertoldi, R. Bondarescu, K. Bongs, P. Bouyer, C. Braxmaier, L. Cacciapuoti, et al., "Stequest—test of the universality of free fall using cold atom interferometry," *Classical and Quantum Gravity* **31**, 115010 (2014).
- <sup>27</sup>S. Abend, M. Gebbe, M. Gersemann, H. Ahlers, H. Muntinga, E. Giese, N. Gaaloul, C. Schubert, C. Lämmerzahl, W. Ertmer, W. P. Schleich, and E. M. Rasel, "Atom-chip fountain gravimeter," *Phys. Rev. Lett.* **117**, 203003 (2016).
- <sup>28</sup>C. Freier, M. Hauth, V. Schkolnik, B. Leykauf, M. Schilling, H. Wziontek, H.-G. Scherneck, J. Müller, and A. Peters, "Mobile quantum gravity sensor with unprecedented stability," in *Journal of Physics: Conference Series*, Vol. 723 (IOP Publishing, 2016) p. 012050.
- <sup>29</sup>Y. Bidel, N. Zahzam, C. Blanchard, A. Bonnin, M. Cadoret, A. Bresson, D. Rouxel, and M. Lequentrec-Lalancette, "Absolute marine gravimetry with matter-wave interferometry," *Nature communications* **9**, 1–9 (2018).
- <sup>30</sup>V. Ménoret, P. Vermeulen, N. Le Moigne, S. Bonvalot, P. Bouyer, A. Landragin, and B. Desruelle, "Gravity measurements below 10<sup>−9</sup> g with a transportable absolute quantum gravimeter," *Scientific reports* **8**, 1–11 (2018).
- <sup>31</sup>X. Wu, Z. Pagel, B. S. Malek, T. H. Nguyen, F. Zi, D. S. Scheirer, and H. Müller, "Gravity surveys using a mobile atom interferometer," *Science advances* **5**, eaax0800 (2019).
- <sup>32</sup>Y. Bidel, N. Zahzam, A. Bresson, C. Blanchard, M. Cadoret, A. V. Olesen, and R. Forsberg, "Absolute airborne gravimetry with a cold atom sensor," *Journal of Geodesy* **94**, 1–9 (2020).
- <sup>33</sup>N. Heine, J. Matthias, M. Sahelgozin, W. Herr, S. Abend, L. Timmen, J. Müller, and E. M. Rasel, "A transportable quantum gravimeter employing delta-kick collimated bose–einstein condensates," *The European Physical Journal D* **74**, 1–8 (2020).
- <sup>34</sup><https://www.muquans.com/>, "Absolute quantum gravimeter," (2022).
- <sup>35</sup>R. Middlemiss, A. Samarelli, D. Paul, J. Hough, S. Rowan, and G. Hammond, "Measurement of the earth tides with a mems gravimeter," *Nature* **531**, 614–617 (2016).
- <sup>36</sup>R. P. Middlemiss, S. G. Bramsiepe, R. Douglas, J. Hough, D. J. Paul, S. Rowan, and G. D. Hammond, "Field tests of a portable mems gravimeter," *Sensors* **17**, 2571 (2017).
- <sup>37</sup>S. Tang, H. Liu, S. Yan, X. Xu, W. Wu, J. Fan, J. Liu, C. Hu, and L. Tu, "A high-sensitivity mems gravimeter with a large dynamic range," *Microsystems & nanoengineering* **5**, 1–11 (2019).
- <sup>38</sup>C. Wang, F. Chen, Y. Wang, S. Sadeghpour, C. Wang, M. Baijot, R. Esteves, C. Zhao, J. Bai, H. Liu, et al., "Micromachined accelerometers with sub- $\mu\text{g}/\sqrt{\text{Hz}}$  noise floor: A review," *Sensors* **20**, 4054 (2020).
- <sup>39</sup>Q. Lu, Y. Wang, X. Wang, Y. Yao, X. Wang, W. Huang, et al., "Review of micromachined optical accelerometers: from mg to sub- $\mu\text{g}$ ," *Opto-Electronic Advances* **4**, 03200045 (2021).
- <sup>40</sup>O. Francis, T. Niebauer, G. Sasagawa, F. Kopping, and J. Gschwind, "Calibration of a superconducting gravimeter by comparison with an absolute gravimeter fg5 in boulder," *Geophysical Research Letters* **25**, 1075–1078 (1998).
- <sup>41</sup>M. Sugihara and T. Ishido, "Geothermal reservoir monitoring with a combination of absolute and relative gravimetry," *Geophysics* **73**, WA37–WA47 (2008).
- <sup>42</sup>D. Crossley, J. Hinderer, and U. Riccardi, "The measurement of surface gravity," *Reports on Progress in physics* **76**, 046101 (2013).
- <sup>43</sup>B. Hector, L. Séguis, J. Hinderer, J.-M. Cohard, M. Wubda, M. Desclotres, N. Benarrosh, and J.-P. Boy, "Water storage changes as a marker for base flow generation processes in a tropical humid basement catchment (b enin): Insights from hybrid gravimetry," *Water Resources Research* **51**, 8331–8361 (2015).
- <sup>44</sup>M. Van Camp, B. Meurers, O. De Viron, and T. Forbriger, "Optimized strategy for the calibration of superconducting gravimeters at the one per mille level," *Journal of Geodesy* **90**, 91–99 (2016).
- <sup>45</sup>P. Abrykosov, R. Pail, T. Gruber, N. Zahzam, A. Bresson, E. Hardy, B. Christophe, Y. Bidel, O. Carraz, and C. Siemes, "Impact of a novel hybrid accelerometer on satellite gravimetry performance," *Advances in Space Research* **63**, 3235–3248 (2019).
- <sup>46</sup>M. Aspelmeyer, T. J. Kippenberg, and F. Marquardt, "Cavity optomechanics," *Reviews of Modern Physics* **86**, 1391 (2014).
- <sup>47</sup>E. Romero, V. M. Valenzuela, A. R. Kermany, L. Sementilli, F. Iacopi, and W. P. Bowen, "Engineering the dissipation of crystalline micromechanical resonators," *Phys. Rev. Applied* **13**, 044007 (2020).
- <sup>48</sup>L. Sementilli, E. Romero, and W. P. Bowen, "Nanomechanical dissipation and strain engineering," *Advanced Functional Materials* **32**, 2105247 (2022).
- <sup>49</sup>W. A. Prothero and J. M. Goodkind, "A superconducting gravimeter," *Review of Scientific Instruments* **39**, 1257–1262 (1968).
- <sup>50</sup>J. M. Goodkind, "The superconducting gravimeter," *Review of Scientific Instruments* **70**, 4131–4152 (1999).
- <sup>51</sup>C. Timberlake, G. Gasbarri, A. Vinante, A. Setter, and H. Ulbricht, "Acceleration sensing with magnetically levitated oscillators above a superconductor," *Applied Physics Letters* **115**, 224101 (2019).
- <sup>52</sup>F. Monteiro, W. Li, G. Afek, C.-I. Li, M. Mossman, and D. C. Moore, "Force and acceleration sensing with optically levitated nanogram masses at microkelvin temperatures," *Phys. Rev. A* **101**, 053835 (2020).
- <sup>53</sup>C. W. Lewandowski, T. D. Knowles, Z. B. Etienne, and B. D'Urso, "High-sensitivity accelerometry with a feedback-cooled magnetically levitated microsphere," *Phys. Rev. Applied* **15**, 014050 (2021).
- <sup>54</sup>S. Qvarfort, A. Serafini, P. F. Barker, and S. Bose, "Gravimetry through non-linear optomechanics," *Nature Communications* **9**, 3690 (2018).
- <sup>55</sup>[https://www.gwrintstruments.com/igrav-gravity\\_sensors.html](https://www.gwrintstruments.com/igrav-gravity_sensors.html), "Superconducting gravity meter," (2022).
- <sup>56</sup>W. Wu, D. Liu, H. Liu, S. Yan, S. Tang, J. Liu, F. Hu, J. Fan, and L. Tu, "Measurement of tidal tilt by a micromechanical inertial sensor employing quasi-zero-stiffness mechanism," *Journal of Microelectromechanical Systems* **29**, 1322–1331 (2020).
- <sup>57</sup>X. Xu, Q. Wang, L. Yang, Y. Fang, Q. Wang, C. Zhao, F. Hu, L. Tu, et al., "On the air buoyancy effect in mems-based gravity sensors for high resolution gravity measurements," *IEEE Sensors Journal* **21**, 22480–22488 (2021).
- <sup>58</sup>S. X. Su, H. S. Yang, and A. M. Agogino, "A resonant accelerometer with two-stage microlleverage mechanisms fabricated by soi-mems technology," *IEEE Sensors Journal* **5**, 1214–1223 (2005).
- <sup>59</sup>A. Tocchio, A. Caspani, and G. Langfelder, "Mechanical and electronic amplitude-limiting techniques in a mems resonant accelerometer," *IEEE Sensors journal* **12**, 1719–1725 (2011).
- <sup>60</sup>A. Mustafazade, M. Pandit, C. Zhao, G. Sobreviela, Z. Du, P. Steinmann, X. Zou, R. T. Howe, and A. A. Seshia, "A vibrating beam mems accelerometer for gravity and seismic measurements," *Scientific reports* **10**, 1–8 (2020).
- <sup>61</sup>J. Zhang, Y. Su, Q. Shi, and A.-P. Qiu, "Microelectromechanical resonant accelerometer designed with a high sensitivity," *Sensors* **15**, 30293–30310 (2015).
- <sup>62</sup>Y. Wang, J. Zhang, Z. Yao, C. Lin, T. Zhou, Y. Su, and J. Zhao, "A mems resonant accelerometer with high performance of temperature based on electrostatic spring softening and continuous ring-down technique," *IEEE Sensors Journal* **18**, 7023–7031 (2018).
- <sup>63</sup>Y. Yin, Z. Fang, Y. Liu, and F. Han, "Temperature-insensitive structure design of micromachined resonant accelerometers," *Sensors* **19**, 1544 (2019).
- <sup>64</sup>Z. Fang, Y. Yin, C. Chen, S. Zhang, Y. Liu, and F. Han, "A sensitive micromachined resonant accelerometer for moving-base gravimetry," *Sensors and Actuators A: Physical* **325**, 112694 (2021).
- <sup>65</sup>G. Langfelder, S. Dellea, F. Zaraga, D. Cucci, and M. A. Urquía, "The dependence of fatigue in microelectromechanical systems on the environment and the industrial packaging," *IEEE Transactions on Industrial Electronics* **59**, 4938–4948 (2011).
- <sup>66</sup>J. Wu, H. Maekoba, A. Parent, and T. Ikehashi, "A sub-1 hz resonance frequency resonator enabled by multi-step tuning for micro-seismometer," *Micromachines* **13**, 63 (2021).
- <sup>67</sup>T. Ikehara and T. Tsuchiya, "Low-cycle to ultrahigh-cycle fatigue lifetime measurement of single-crystal-silicon specimens using a microresonator test device," *Journal of Microelectromechanical Systems* **21**, 830–839 (2012).
- <sup>68</sup>V. Belwanshi, A. Prasad, K. Toland, R. Middlemiss, D. Paul, and G. Hammond, "Investigation of temperature sensitivity of a mems gravimeter based on geometric anti-spring," *Review of Scientific Instruments* **93**, 125002 (2022).

- <sup>69</sup>C. M. Jha, M. A. Hopcroft, S. A. Chandorkar, J. C. Salvia, M. Agarwal, R. N. Candler, R. Melamud, B. Kim, and T. W. Kenny, "Thermal isolation of encapsulated mems resonators," *Journal of Microelectromechanical Systems* **17**, 175–184 (2008).
- <sup>70</sup>J. C. Salvia, R. Melamud, S. A. Chandorkar, S. F. Lord, and T. W. Kenny, "Real-time temperature compensation of mems oscillators using an integrated micro-oven and a phase-locked loop," *Journal of Microelectromechanical Systems* **19**, 192–201 (2010).
- <sup>71</sup>J. Lee and J. Rhim, "Temperature compensation method for the resonant frequency of a differential vibrating accelerometer using electrostatic stiffness control," *Journal of Micromechanics and Microengineering* **22**, 095016 (2012).
- <sup>72</sup>C.-S. Liu, R. Tabrizian, and F. Ayazi, "A  $\pm 0.3$  ppm oven-controlled mems oscillator using structural resistance-based temperature sensing," *IEEE Transactions on Ultrasonics, Ferroelectrics, and Frequency Control* **65**, 1492–1499 (2018).
- <sup>73</sup>A. Hajjam, A. Logan, and S. Pourkamali, "Doping-induced temperature compensation of thermally actuated high-frequency silicon micromechanical resonators," *Journal of Microelectromechanical Systems* **21**, 681–687 (2012).
- <sup>74</sup>A. K. Samrao and F. Ayazi, "Temperature compensation of silicon resonators via degenerate doping," *IEEE Transactions on Electron Devices* **59**, 87–93 (2012).
- <sup>75</sup>R. Melamud, S. A. Chandorkar, B. Kim, H. K. Lee, J. C. Salvia, G. Bahl, M. A. Hopcroft, and T. W. Kenny, "Temperature-insensitive composite micromechanical resonators," *Journal of Microelectromechanical Systems* **18**, 1409–1419 (2009).
- <sup>76</sup>R. Tabrizian, G. Casinovi, and F. Ayazi, "Temperature-stable silicon oxide (silox) micromechanical resonators," *IEEE Transactions on Electron Devices* **60**, 2656–2663 (2013).
- <sup>77</sup>C. Comi, A. Corigliano, G. Langfelder, A. Longoni, A. Tocchio, and B. Simoni, "A resonant microaccelerometer with high sensitivity operating in an oscillating circuit," *Journal of microelectromechanical systems* **19**, 1140–1152 (2010).
- <sup>78</sup>U. Park, J. Rhim, J. U. Jeon, and J. Kim, "A micromachined differential resonant accelerometer based on robust structural design," *Microelectronic Engineering* **129**, 5–11 (2014).
- <sup>79</sup>M. Pandit, C. Zhao, G. Sobreviela, and A. Seshia, "Practical limits to common mode rejection in mode localized weakly coupled resonators," *IEEE Sensors Journal* **20**, 6818–6825 (2019).
- <sup>80</sup>H. Kang, B. Ruan, Y. Hao, and H. Chang, "A mode-localized resonant accelerometer with self-temperature drift suppression," *IEEE Sensors Journal* **20**, 12154–12165 (2020).
- <sup>81</sup>N. Zen, T. A. Puurtinen, T. J. Isotalo, S. Chaudhuri, and I. J. Maasilta, "Engineering thermal conductance using a two-dimensional phononic crystal," *Nature communications* **5**, 1–9 (2014).
- <sup>82</sup>M. Maldovan, "Phonon wave interference and thermal bandgap materials," *Nature materials* **14**, 667–674 (2015).
- <sup>83</sup>J. Maire, R. Anufriev, R. Yanagisawa, A. Ramiere, S. Volz, and M. Nomura, "Heat conduction tuning by wave nature of phonons," *Science advances* **3**, e1700027 (2017).
- <sup>84</sup>X. Zhang, X. Wei, Y. Gao, M. Zhao, Y. Qi, L. Zhao, and Z. Jiang, "A tunable quasi-zero stiffness mechanism for thermal compensation of a mems gravimeter," *Conference: 2021 IEEE 16th International Conference on Nano/Micro Engineered and Molecular Systems (NMES)* (2021), <https://doi.org/10.1109/NMES51315.2021.9451277>.
- <sup>85</sup>C. Bourgeois, J. Hermann, N. Blanc, N. de Rooij, and F. Rudolf, "Determination of the elastic temperature coefficients of monocrystalline silicon," *In Proceedings of the International Solid-State Sensors and Actuators Conference* (2013).
- <sup>86</sup>H. Liu, W. Pike, C. Charalambous, and A. E. Stott, "Passive method for reducing temperature sensitivity of a microelectromechanical seismic accelerometer for marsquake monitoring below 1 nano-g," *Physical review applied* **12**, 064057 (2019).
- <sup>87</sup>C. Hirt, S. Claessens, T. Fecher, M. Kuhn, R. Pail, and M. Rexer, "New ultrahigh-resolution picture of earth's gravity field," *Geophysical research letters* **40**, 4279–4283 (2013).
- <sup>88</sup>Y. T. Yang, K. L. Ekinci, X. M. H. Huang, L. M. Schiavone, M. L. Roukes, C. A. Zorman, and M. Mehregany, "Monocrystalline silicon carbide nanoelectromechanical systems," *Applied Physics Letters* **78**, 162–164 (2001).
- <sup>89</sup>A. R. Kermany, J. S. Bennett, V. M. Valenzuela, W. P. Bowen, and F. Iacopi, "Potential of epitaxial silicon carbide microbeam resonators for chemical sensing," *physica status solidi (a)* **214**, 1600437 (2017).
- <sup>90</sup>P. S. Timoshenko, "X. on the transverse vibrations of bars of uniform cross-section," *The London, Edinburgh, and Dublin Philosophical Magazine and Journal of Science* **43**, 1 (1901).
- <sup>91</sup>T. Huang, "The effect of rotatory inertia and of shear deformation on the frequency and normal mode equations of uniform beams with simple end conditions," *Journal of Applied Mechanics* **28**, 579–584 (1961).
- <sup>92</sup>K. Brueckner, F. Niebelschuetz, K. Tonisch, C. Foerster, V. Cimalla, R. Stephan, J. Pezoldt, T. Stauden, O. Ambacher, and M. A. Hein, "Micro- and nano-electromechanical resonators based on sic and group iii-nitrides for sensor applications," *physica status solidi (a)* **208**, 357–376 (2011).
- <sup>93</sup>V. Belwanshi, A. Prasad, K. Toland, R. Middlemiss, D. J. Paul, and G. D. Hammond, "Investigation of temperature sensitivity of a mems gravimeter based on geometric anti-spring," *Rev. Sci. Instrum.* **93**, 125002 (2022).
- <sup>94</sup>J. Qiu, J. Lang, and A. Slocum, "A curved-beam bistable mechanism," *J. Microelectromech. S.* **13**, 137 (2004).
- <sup>95</sup>H. Watanabe, N. Yamada, and M. Okaji, "Linear thermal expansion coefficient of silicon from 293 to 1000 k," *International journal of thermophysics* **25**, 221–236 (2004).
- <sup>96</sup>E. Boyd, L. Li, R. Blue, and D. Uttamchandani, "Measurement of the temperature coefficient of young's modulus of single crystal silicon and 3c silicon carbide below 273 k using micro-cantilevers," *Sensor Actuat. A* **198**, 75 (2013).
- <sup>97</sup>S. S. Hakaru Masumoto, "Thermal expansion coefficient and the temperature coefficient of young's modulus of cobalt and palladium alloys," *Transactions of the Japan Institute of Metals* **11**, 91–93 (1970).
- <sup>98</sup>T. K. Hakaru Masumoto, Hideo Saitō, "The thermal expansion coefficients and the temperature coefficients of young's modulus of the alloys of iron and palladium," *Transactions of the Japan Institute of Metals* **4**, 114–117 (1963).
- <sup>99</sup>S. S. Hakaru Masumoto, Hideo Saitō, "Thermal expansion and temperature dependence of young's modulus of nickel-copper alloys," *Transactions of the Japan Institute of Metals* **11**, 88–90 (1970).
- <sup>100</sup>T. K. Hakaru Masumoto, "On the thermal expansion coefficient and the temperature coefficient of young's modulus of iron-platinum alloys," *Transactions of the Japan Institute of Metals* **6**, 113–115 (1965).
- <sup>101</sup>S. S. Hakaru Masumoto, "The thermal expansion coefficient and the temperature coefficient of young's modulus of nickel-palladium and nickel-platinum alloys," *Transactions of the Japan Institute of Metals* **11**, 391–394 (1970).
- <sup>102</sup>M. G. Holland, "Analysis of lattice thermal conductivity," *Phys. Rev.* **132**, 2461–2471 (1963).
- <sup>103</sup>C. J. Glassbrenner and G. A. Slack, "Thermal conductivity of silicon and germanium from 3°k to the melting point," *Phys. Rev.* **134**, A1058–A1069 (1964).
- <sup>104</sup>T. B. Gabrielson, "Mechanical-thermal noise in micromachined acoustic and vibration sensors," *IEEE transactions on Electron Devices* **40**, 903–909 (1993).
- <sup>105</sup>H. Abe, H. Kato, and T. Baba, "Specific heat capacity measurement of single-crystalline silicon as new reference material," *Japanese Journal of Applied Physics* **50**, 11RG01 (2011).
- <sup>106</sup>W. Weaver Jr, S. P. Timoshenko, and D. H. Young, *Vibration problems in engineering* (John Wiley & Sons, 1991).
- <sup>107</sup>S. P. Timoshenko, "The shear coefficient in timoshenko's beam theory," *Journal of Mechanics* **32**, 515–518 (2016).
- <sup>108</sup>G. Cowper, "The shear coefficient in timoshenko's beam theory," *Journal of Mechanics* **32**, 515–518 (2016).
- <sup>109</sup>L. Landau, E. Lifšic, E. Lifshitz, A. Kosevich, J. Sykes, L. Pitaevskii, and W. Reid, *Theory of Elasticity: Volume 7, Course of theoretical physics* (Elsevier Science, 1986).
- <sup>110</sup>K. M. Goeders, J. S. Colton, and L. A. Bottomley, "Microcantilevers: sensing chemical interactions via mechanical motion," *Chemical reviews* **108**, 522–542 (2008).
- <sup>111</sup>N. Kuramoto, L. Zhang, S. Mizushima, A. Waseda, S. Okubo, H. Inaba, A. Kurokawa, and K. Fujii, "Absolute measurement of the density of silicon spheres to improve the primary density standard of nmij," *Metrologia* **57**, 025006 (2020).
- <sup>112</sup>M. A. Hopcroft, W. D. Nix, and T. W.

- Kenny, “What is the young’s modulus of silicon?” *Journal of Microelectromechanical Systems* **19**, 229–238 (2010).
- <sup>113</sup>J. Vanhellemont, A. K. Swarnakar, and O. Van der Biest, “Temperature dependent young’s modulus of si and ge,” *ECS Transactions* **64**, 283 (2014).
- <sup>114</sup>J. F. Nye et al., “Physical properties of crystals: their representation by tensors and matrices,” Oxford university press, pp. 131 (1985).
- <sup>115</sup>K. Lyon, G. Salinger, C. Swenson, and G. White, “Linear thermal expansion measurements on silicon from 6 to 340 k,” *Journal of Applied Physics* **48**, 865–868 (1977).
- <sup>116</sup>W. M. Haynes, D. R. Lide, and T. J. Bruno, *CRC handbook of chemistry and physics* (CRC press, 2016).
- <sup>117</sup>G. A. Slack and S. F. Bartram, “Thermal expansion of some diamondlike crystals,” *Journal of Applied Physics* **46**, 89–98 (1975).
- <sup>118</sup>R. Roberts, “Thermal expansion reference data: silicon 300–850 k,” *Journal of Physics D: Applied Physics* **14**, L163 (1981).
- <sup>119</sup>C. Swenson, “Recommended values for the thermal expansivity of silicon from 0 to 1000 k,” *Journal of physical and chemical reference data* **12**, 179–182 (1983).
- <sup>120</sup>G. White and M. Minges, “Thermophysical properties of some key solids: an update,” *International Journal of Thermophysics* **18**, 1269–1327 (1997).
- <sup>121</sup>T. Middelmann, A. Walkov, G. Bartl, and R. Schödel, “Thermal expansion coefficient of single-crystal silicon from 7 k to 293 k,” *Physical Review B* **92**, 174113 (2015).
- <sup>122</sup>NIST, “Material properties: Silicon,” <https://trc.nist.gov/cryogenics/materials/Silicon/Silicon.htm>.
- <sup>123</sup>R. Schoedel and G. Boensch, In *Recent Developments in Traceable Dimensional Measurement*.
- <sup>124</sup>P. B. Karlmann, K. Klein, P. Halverson, R. Peters, M. Levine, D. Van Buren, and M. Dudik, in *AIP Conference Proceedings*, Vol. 824 (American Institute of Physics, 2006) pp. 35–42.
- <sup>125</sup>G. Bartl, C. Elster, J. Martin, R. Schödel, M. Voigt, and A. Walkov, “Thermal expansion and compressibility of single-crystal silicon between 285 k and 320 k,” *Measurement Science and Technology* **31**, 065013 (2020).
- <sup>126</sup>J. Wortman and R. Evans, “Young’s modulus, shear modulus, and poisson’s ratio in silicon and germanium,” *Journal of applied physics* **36**, 153–156 (1965).
- <sup>127</sup>J. J. Hall, “Electronic effects in the elastic constants of n-type silicon,” *Physical Review* **161**, 756 (1967).
- <sup>128</sup>E. J. Boyd and D. Uttamchandani, “Measurement of the anisotropy of young’s modulus in single-crystal silicon,” *Journal of Microelectromechanical Systems* **21**, 243–249 (2011).
- <sup>129</sup>J. Wachtman Jr, W. Tefft, D. Lam Jr, and C. Apstein, “Exponential temperature dependence of young’s modulus for several oxides,” *Physical review* **122**, 1754 (1961).